Research Repository UCD

Title	Cortical network effects of subthalamic deep brain stimulation in a thalamo-cortical microcircuit model
Authors(s)	Farokhniaee, AmirAli, Lowery, Madeleine M.
Publication date	2021-04-06
Publication information	Farokhniaee, AmirAli, and Madeleine M. Lowery. "Cortical Network Effects of Subthalamic Deep Brain Stimulation in a Thalamo-Cortical Microcircuit Model." IOP Publishing, April 6, 2021. https://doi.org/10.1088/1741-2552/abee50.
Publisher	IOP Publishing
Item record/more information	http://hdl.handle.net/10197/26346
Publisher's statement	Original content from this work may be used under the terms of the Creative Commons Attribution 4.0 license. Any further distribution of this work must maintain attribution to the author(s) and the title of the work, journal citation and DOI.
Publisher's version (DOI)	10.1088/1741-2552/abee50

Downloaded 2026-05-02 00:25:05

The UCD community has made this article openly available. Please share how this access benefits you. Your story matters! (@ucd_oa)

© Some rights reserved. For more information

Journal of Neural Engineering

PAPER • **OPEN ACCESS**

Cortical network effects of subthalamic deep brain stimulation in a thalamo-cortical microcircuit model

To cite this article: AmirAli Farokhniaee and Madeleine M Lowery 2021 *J. Neural Eng.* **18** 056006

View the article online for updates and enhancements.

This content was downloaded from IP address 84.203.41.231 on 14/04/2021 at 08:45

Journal of Neural Engineering

OPEN ACCESS

RECEIVED
12 January 2021

REVISED
18 February 2021

ACCEPTED FOR PUBLICATION
12 March 2021

PUBLISHED
6 April 2021

Original content from this work may be used under the terms of the Creative Commons Attribution 4.0 licence.

Any further distribution of this work must maintain attribution to the author(s) and the title of the work, journal citation and DOI.

PAPER

Cortical network effects of subthalamic deep brain stimulation in a thalamo-cortical microcircuit model

AmirAli Farokhniaee* and **Madeleine M Lowery**

Neuromuscular Systems Lab, School of Electrical & Electronic Engineering, University College Dublin, Dublin, Ireland

* Author to whom any correspondence should be addressed.

E-mail: amirali.farokhniaee@ucd.ie

Keywords: antidromic, deep brain stimulation, motor cortex, Parkinson's disease, computational model, beta rhythm, thalamocortical microcircuit

Supplementary material for this article is available online

Abstract

Objective. High frequency deep brain stimulation (DBS) of the subthalamic nucleus (STN) suppresses excessive beta band (∼13–30 Hz) activity of the motor cortex in Parkinson's disease (PD). While the mechanisms of action of STN DBS are not well-understood, strong evidence supports a role for cortical network modulating effects elicited by antidromic activation of cortical axons via the hyperdirect pathway. *Approach*. A spiking model of the thalamo-cortical microcircuit was developed to examine modulation of cortical network activity by antidromic STN DBS, mediated by direct activation of deep pyramidal neurons (PNs) and subsequent indirect activation of other thalamo-cortical structures. *Main results*. Increasing synaptic coupling strength from cortical granular to superficial layers, from inhibitory neurons to deep PNs, and from thalamus reticular to relay cells, along with thalamocortical connection strength, accompanied by reduced coupling from cortical superficial to granular layers, from thalamus relay cells to reticular neurons, and corticothalamic connection strength, led to increased beta activity and neural synchrony, as observed in PD. High frequency DBS desynchronized correlated neural activity, resulting in clusters of both excited and inhibited deep cortical PNs. The emergence of additional frequency components in the local field potential (LFP), and increased power at subharmonics of the DBS frequency as observed in patients with dyskinesia during DBS, occurred under different stimulus amplitudes and frequencies. While high-frequency (>100 Hz) DBS suppressed the LFP beta power, low-frequency (<40 Hz) DBS increased beta power when more than 10% of PNs were activated, but reduced the total beta power at lower levels of neural activation. *Significance*. The results suggest a potential mechanism for experimentally observed alterations in cortical neural activity during DBS via the propagation of DBS stimuli throughout the cortical network, modulated by short-term synaptic plasticity, and the emergence of resonance due to interaction of DBS with existing M1 rhythms by engaging feedforward-feedback loops.

1. Introduction

Neurophysiological changes associated with Parkinson's disease (PD) and dopaminergic neurodegeneration have a critical effect on the functioning of cortical networks involved in motor command and execution, including the primary motor cortex (M1) [1]. Examples of altered cortical network activity in PD, include exaggerated beta-band oscillations (∼13–30 Hz) observed in local field potential (LFP) recordings from cortical deep layers in rats [2] and electrocorticography recordings in awake rats [3] and PD patients [4, 5]. M1 LFP recordings in PD patients have revealed increased beta band oscillations during the stop-phase of movement [6], even in the early stages of the disease [7]. In addition, bursts of neural activity with long periods of silence are observed in the LFP recordings of M1 along with wide-spread synchronization between neural spike trains [2]. This wide-spread synchronization has been shown to be related to alterations in the strength of neuronal coupling in the cortical motor network [8]. In

© 2021 The Author(s). Published by IOP Publishing Ltd

addition, alterations in interconnections within and between neurons in layer V of the motor cortex and interneurons are believed to play a role in the elevated synchrony observed within the parkinsonian motor cortex network [9]. Alterations in neuronal activity in the motor cortex is paralleled by changes in motor function and has been implicated in the etiology of parkinsonian motor symptoms [10].

The origin of enhanced beta oscillations observed throughout the cortex and basal ganglia (BG) in PD, and the role of the cortex in their generation and maintenance, is not yet fully understood. Computational and animal models have indicated that excessive beta rhythm can emerge within the striatum as well as within the reciprocally connected subthalamic nucleus (STN)—globus pallidus external (GPe) network [11–13]. Alteration of neuronal coupling also gives rise to wide-spread increased synchronization of neuronal activity throughout the cortico-thalamic-BG network in PD, as captured in computational modelling studies [14, 15]. Exaggerated beta oscillations are strongest among neurons in the deep layers of M1 that project to the BG and have been considered as a potential source of beta generation in M1 [16]. An intermediate view hypothesizes that beta rhythms emerge in the neocortex through interactions between laminar layers, but depend on external synaptic drive, potentially from the BG or thalamus [17]. In a recent study, Reis *et al* employed dynamic causal modelling to identify the connection topology that best explained the transition between low levels of beta rhythm (low beta) and high levels of beta rhythm (high beta) generation in M1 among a set of neural mass models of the thalamo-cortex [18]. Their model suggests that high levels of cortical beta synchrony may arise as a result of extrinsic input from thalamocortical (TC) relay cells to deep pyramidal cells combined with increased input from middle pyramidal cells to superficial pyramidal ones.

Therapeutic deep brain stimulation (DBS) of the STN disrupts pathological beta activity and has been shown to alter cortical motor network activity, inducing widespread and heterogeneous network effects [8]. In addition to orthodromic effects of DBS on cortical activity via the globus pallidum [15, 19], antidromic activation of layer V pyramidal neurons (PNs) via the hyperdirect pathway has been demonstrated to modulate cortical excitability and network information processing, including suppression of slow-wave and beta oscillations [20–23]. Simulation studies have similarly demonstrated suppression of beta band oscillations within the cortex and STN through antidromic activation of STN afferent inputs [24] and robust antidromic propagation of action potentials to the cortex in detailed models of hyperdirect neurons [25]. The relative contribution of antidromic activation to the therapeutic effects of DBS, however, is not yet known. Optogenetic studies have shown that activation of the hyperdirect pathway is sufficient, though not necessary, to ameliorate parkinsonian symptoms in rodent models [26, 27]. Antidromic activation of STN DBS in primate models has also been shown to vary across subjects and over time, while therapeutic effects were maintained [28]. In addition to the relative contribution of antidromic effects to the therapeutic efficacy of DBS, given the central role of the cortex in the control of motor function, it is critical to understand the impacts of DBS on the cortical network activity.

Alterations in cortical neural activity during DBS in 6-OHDA-lesioned rats and PD patients include the partial entrainment of cortical neurons, suppression of beta band M1 LFP oscillations, attenuation of cortical beta rhythm hypersynchrony and reduced synchronized activity among layer V neurons [2, 5]. A peak in gamma band activity at subharmonics of the stimulation frequency has also been observed in patients with DBS-induced dyskinesia [29]. Collectively, these studies indicate that STN DBS induces substantial changes in cortical neural activity in patients and animal models. Given the central role of the cortex in the control of motor function, an understanding of how DBS alters neural activity within the cortical network is critical in understanding the mechanism by which DBS exerts its therapeutic effects and its impact on cortical information processing.

With limited simultaneous recordings across the network possible with experimental methods, computational modelling provides a powerful means to explore the influence of DBS throughout the thalamo-cortical network. Computational modelling has been extensively used to examine the effect of DBS on the STN-GPe network and, using simplified representations of the thalamus and cortex, on the cortcio-BG network [15, 24, 30, 31]. The effect of antidromic invasion of the laminar cortical network during DBS and on the emergence of beta oscillatory activity through TC interactions, however, has not yet been examined using *in silico* models. To address this, the aim of this study was to develop a thalamo-cortical microcircuit (TCM) model of spiking neurons that captures cortical network effects of DBS during PD-like conditions. The model allows direct comparison with neural firing patterns and LFPs recorded experimentally and is used as a framework to study cortical network effects of antidromic activation of the hyperdirect pathway during STN DBS, in particular the suppression of excessive beta rhythms and alterations in neural synchrony. Using the model, it is possible to examine the effects of antidromic activation of cortical neurons in isolation without the confounding influence of orthodromic activation. In this way, the different pathways stimulated during DBS and the resulting changes in network activity can be deconstructed. In addition to providing insight into the mechanisms of DBS, this

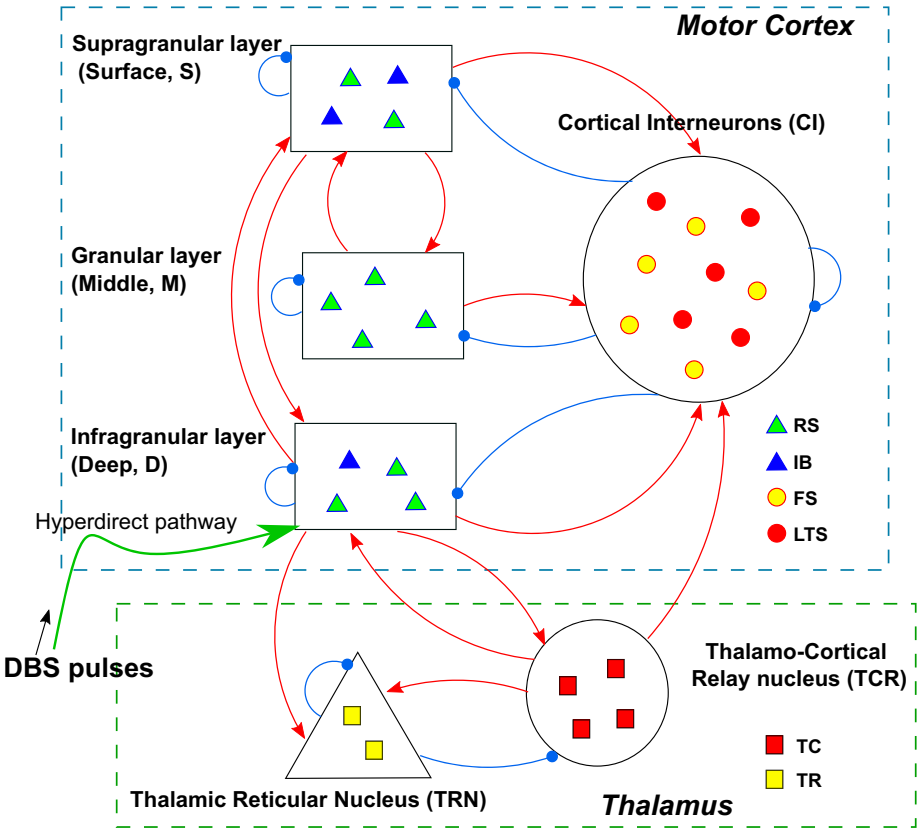

Figure 1. Schematic diagram of the TCM model with the addition of STN DBS. The population consists of regular spiking (RS), intrinsically bursting (IB), fast spiking (FS), low-threshold spiking (LTS), thalamocortical (TC) and thalamic reticular (TR) neurons. Excitatory and inhibitory connetions are shown with red and blue curves, respectively.

approach may enable the identification of alternative less-invasive targets for stimulation.

2. Materials and methods

2.1. TCM spiking neural network model

A spiking neuronal population model of the TCM, comprised of an ensemble of point-like Izhikevich neurons, was developed (figure 1). The model was motivated by alterations in synaptic coupling strength within, and between, the motor cortex and thalamus identified using dynamic causal modelling in parkinsonian rats by Reis *et al* [18].

The overall structure of the spiking TCM model is based upon the neural mass model of the TC circuit presented in [18], which itself originated as a combination of two distinct models of the motor cortex (adapted for the motor cortex from the sensory cortex [32–34]) and thalamus [35, 36]. Representation of the cortex as a three-layer structure in combination with the thalamus consisting of two distinct nuclei has been extensively used to understand population phenomena in TC neuronal ensembles including the emergence of neural oscillations [37]. The TCM model presented here consists of 540 point-like spiking neurons that were modeled using Izhikevich spiking neurons [38] and span different layers of the cortex and nuclei of thalamus (figure 1). The Izhikevich model of spiking neurons originated from cortical rat models and is widely accepted as a computationally efficient model of neural activity that captures many of the complex natural spiking phenomena exhibited by real neurons. The excitatory populations of PNs in the primary motor cortex were segregated into three layers: supragranular or surface (S), granular or middle (M) and infragranular or deep (D). They share one common population of cortical inhibitory neurons (CI). The excitatory neurons in the thalamus form the thalamocortical relay nucleus (TCR) and the inhibitory neurons comprise the thalamic reticular nucleus (TRN). Cortical populations contain subpopulations of different neuron types. These subpopulations were incorporated by changing the parameters of the Izhikevich model to exhibit different intrinsic spiking patterns. PN parameters in the cortex were set to generate regular spiking and intrinsically bursting behavior. CIs were subdivided into fast spiking and low-threshold spiking neurons. TCR and TRN nuclei contain TC and thalamic reticular (TR) types, respectively, with no subpopulations. The parameter values for all neurons are provided in the supplementary material, table S1 (available online at stacks.iop.org/JNE/18/056006/mmedia). We incorporated the 3–1 ratio of the number of excitatory and inhibitory neurons in the cortex as well as stronger inhibitory synapses, in line with the

common modelling approach in cortical circuits [35]. There are 100 neurons considered in each population except TRN that contains 40 neurons. The distribution of the subpopulations is summarized in table S2, supplementary material.

All synaptic connections were modeled using Tsodyks–Markram (TM) synapses [39, 40] with parameter values given in the supplementary material, table S3. Two corticothalamic pathways projecting from D to TCR and TRN model the synaptic connections between the cortex and the thalamus. Reciprocally, two TC extrinsic synaptic connections are considered from TCR to both D and CI [35]. There is no connection between TC neurons within TCR and all to all connections exist for TR neurons in TRN [35]. The synaptic connections between the neurons were considered as a combination of Facilitating (F), Depressing (D) and Pseudo-linear (P) synapses with parameters and population distribution as detailed in table S3 of the supplementary material. However, there were two exceptions; the synaptic connections between layer D of the motor cortex and thalamus were considered pure facilitating and between TCR and layer D were set as pure depressing [35]. The synaptic connectivity strengths were distributed in a uniform random manner, with average normalized values as given in figure S1 of the supplementary material, which were identified as leading to generation of elevated cortical beta rhythm in the TCM.

Antidromic activation of deep layer cortical afferents projecting to the STN during STN DBS was incorporated within the model. The electric field generated during DBS can stimulate the hyperdirect neurons axon collaterals that project to the STN, resulting in antidromic activation of deep layer PNs [2, 23, 25, 41]. These induced intracellular membrane currents were considered as Dirac delta functions in the first approximation, which were added intercellularly to the point-like Izhikevich neurons:

$$I_{\mathrm{dbs}}(t) = A\sum_{t'=0}^{T}\delta(t-t');t' = 0,\frac{1}{f_{\mathrm{dbs}}},\frac{2}{f_{\mathrm{dbs}}},\ldots,T \tag{1}$$

where $I_{\mathrm{dbs}}(t)$ is the induced intracellular membrane current, A is a constant that defines the amplitude of the Dirac delta function $\delta(t-t')$, t' is the pulse event time that repeats every period of DBS, f_{dbs} is the DBS stimulation frequency and T is the total time that DBS is on. In other words, I_{dbs} is zero at all times except at the time of occurrence of the stimulation pulse with amplitude A.

The various pathways by which DBS directly and indirectly activates the TCM are illustrated schematically in figure 2. The DBS-induced action potentials (symbolized as pink vertical lines in figure 2) directly activate a percentage of PNs in the deep layer of M1 (green path in figure 2). Consequently, these DBS pulses spread throughout the TC microcircuit by means of synaptic contacts such as axon-axonal and axon-dendritic contact points (the pink pulses with declining amplitude in figure 2). This formalism has been utilized to investigate the effect of DBS postsynaptic pulses on a single neuron firing activity [42] and is extended here to a network level. To represent all these types of connections, we assumed the percentage of neurons in the other populations that make contact with the hyperdirect neurons activated during DBS is the same as the percentage of PNs in layer D that are directly activated by DBS. For example, if the amplitude of DBS is set to activate 25% of the PNs in layer D directly, then 25% of the postsynaptic connections in layer S, CI, TCR and TRN receive these pulses indirectly after passing through TM synapses (see figure 2).

The overall network dynamics of the TCM is described by equations (2) and (3) and reset condition (4). For each structure of the TCM model, $j = 1$, 2, 3, 4, 5, 6 corresponds to the structures S, M, D, CI, TRN and TCR, respectively. For each neuron $i = 1$, 2, …, N_j in structure j (where N_j is the total number of neurons in the corresponding layer j) the neuron fires once its membrane voltage, v_{ij}, reaches threshold and immediately reset to the initial value based on equations (2) and (3) and reset condition (4):

$$\begin{aligned}\dot{v}_{ij} = {} & 0.04v_{ij}^2 + 5v_{ij} - u_{ij} + 140 + I_{ij} \\ & + \sum_{j,j'=1}^{6}\sum_{i,i'=1}^{N_j}\omega_{i'j',ij}\,\mathrm{PSC}_{i'j'}\left(t - \Delta_{j,j'}\right) \\ & + \sum_{k,t_k}\mu_{jk}\,\delta(t-t_k) + \xi(t) + I_{\mathrm{dbs}}\delta_{j3}\end{aligned} \tag{2}$$

$$\dot{u}_{ij} = a_{ij}\left(b_{ij}v_{ij} - u_{ij}\right) \tag{3}$$

$$\text{if } v_{ij} \geqslant v_{p_{ij}} + \zeta(t) \text{ then } v_{ij} \leftarrow c_{ij} \text{ and } u_{ij} \leftarrow u_{ij} + d_{ij} \tag{4}$$

with the auxiliary after-spike if statement for resetting. Here u_{ij} represents the membrane recovery variable, where a_{ij} and b_{ij} are its time scale and sensitivity to the subthreshold fluctuations of v_{ij}, respectively. c_{ij} and d_{ij} describe the after-spike reset value of v_{ij} and u_{ij}, respectively. The TCM model was designed as a suprathreshold, noise-driven spiking neural network. The values of external direct input I (the bias currents) to neuron i in structure j is set such that it is just above the firing threshold and the addition of white gaussian noise, $\xi(t)$, to the membrane current of each individual neuron adjusts the mean firing rates compatible with experimental recordings [2]. $\zeta(t)$ is a Gaussian white noise added to individual neurons threshold potentials. The mean of this threshold noise was set to half of the additive white gaussian noise. Equation (2) is formulated such that the DBS-induced intracellular transmembrane current (I_{dbs}) is added only to Layer D ($j = 3$) by means

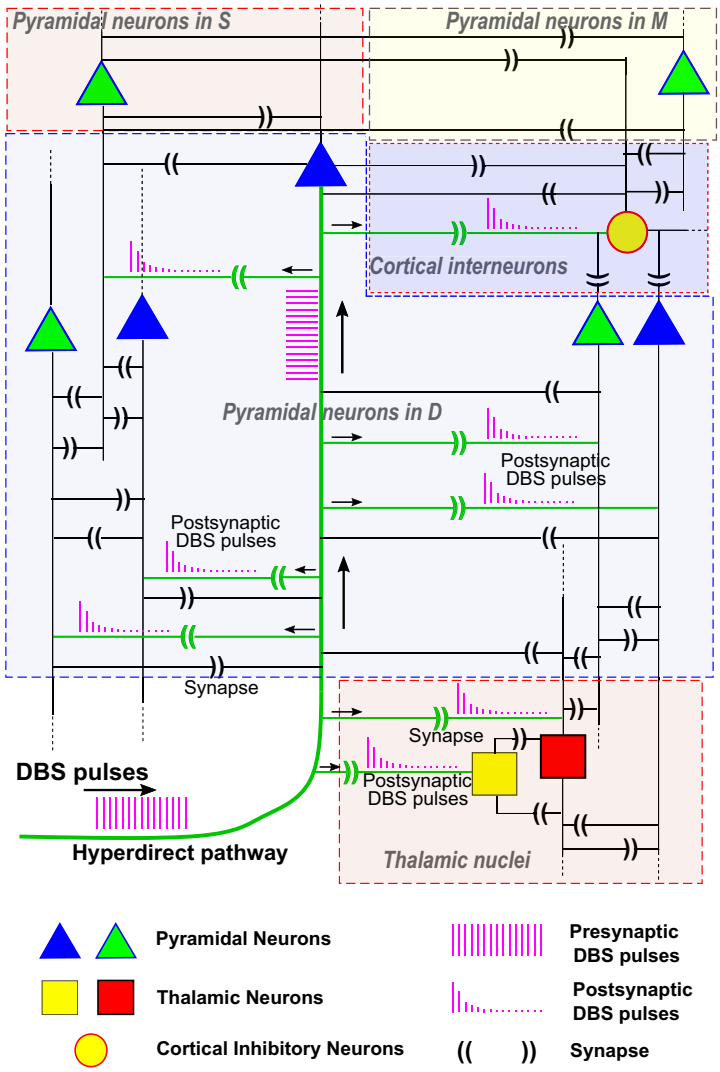

Figure 2. Schematic diagram of the TCM illustrating propagation of DBS pulses through the network via the hyperdirect pathway and synapses. Only some of the many synaptic connections are illustrated. The synaptic connectivity strengths are distributed in a uniform random manner.

of the Kronecker delta function (δ_{j3}). Note that this is an event-driven point-neuron model and does not consider the axonal and dendritic geometry. Postsynaptic currents (PSCs) form all other neurons are added to each neuron in the model by means of a weighting matrix that its elements form the terms ω_{ij}. This matrix contains random elements for the non-zero connections. In other words, this network contains all-to-all random synaptic connections that delivers the PSCs to the neurons in the network (see supplementary materials for more detail). Weak background noise for all layers and nuclei of the TCM was modelled as a Poisson process represented by the term $\sum_{k,t_k} \mu_{jk}\,\delta(t-t_k)$ in equation (2), with inputs occurring at time t_k within each structure. As the LFP primarily reflects synaptic activity among populations of neurons in the vicinity of the recording electrode, and the LFP is dominated by neurons with synaptic processes in the recording layer [43], layer V cortical LFPs were simulated as the sum of all excitatory PSCs (EPSCs) within layer D and the overall CI PSCs scaled by the conductivity of the surrounding grey matter, σ, and the distance between the recording electrode and each neuron, r,as in equation (5):

$$\mathrm{LFP}(t) = \frac{1}{4\pi\sigma r}\left(\sum_{i=1}^{N_3}\mathrm{EPSC}_i(t) + \sum_{i=1}^{N_4}\mathrm{IPSC}_i(t)\right). \tag{5}$$

Considering grey matter with $\sigma \approx 0.27\ (\mathrm{S\ m})^{-1}$ [44] and assuming $r = 100\ \mu$m [43] for all neurons.

Both synaptic and axonal transmission delays were considered in the TCM model. A synaptic transmission time delay of 1 ms was set along all synapses in the microcircuit. The PSCs transmission delay is 8 ms between different structures within the motor cortex and thalamus ($\Delta_{j,j'} = 8$ ms for $j \neq j'$), and 1 ms within each structure ($\Delta_{j,j'} = 1$ ms for $j = j'$) [18]. The transmission delay from layer D of the cortex to thalamus (corticothalamic delay) was set to 15 ms ($\Delta_{3,5} = \Delta_{3,6} = 15$ ms) while in the opposite path

(TC delay) was equal to 20 ms ($\Delta_{6,3} = \Delta_{6,4} = 20$ ms) [45]. Note that different synaptic and axonal time delays have significant effects on the frequency of the dominant oscillations, hence their alterations yield to production of various rhythms and shifting the existing rhythms within the system.

2.2. Data analysis

The correlation index (an indicative of the degree of correlation) was estimated as the maximum value of the normalized cross correlation between the spike trains representing the firing times of pairs of neurons. The magnitude and phase of spike-spike coherences were calculated using the Chronux software package [46] for Matlab that utilizes multi-taper coherence method in point process time series. Suppressed and excited states of deep PNs during DBS were defined as spike trains with mean firing rates greater and less than the mean firing rates during DBS off, respectively. Power spectral densities (PSDs) throughout the whole paper were estimated using Welches' method for overlapping windows of 500 ms. To examine the effect of DBS amplitude and frequency on subharmonics at half the DBS frequency, at each frequency of DBS, we varied the amplitude of the intercellularly injected DBS current (A) and calculated the integral of the resulting PSD in the range ± 5 Hz around half of the DBS stimulation frequency, f_{dbs}, as both amplitude and frequency were varied:

$$P = \int_{\frac{f_{\mathrm{dbs}}-10}{2}}^{\frac{f_{\mathrm{dbs}}+10}{2}} \mathrm{PSD}\,(f)\ \mathrm{d}f. \tag{6}$$

The beta power was defined as the area under the PSD curve between 13 and 30 Hz. The data were analyzed in Matlab 2018a using custom developed codes, unless otherwise stated.

2.3. Simulation details

Simulations were conducted at room temperature with 0.1 ms time step in Matlab 2018a (The Mathworks, Inc.) using the Euler method on an Intel® Core™ i7-8700 CPU @ 3.2 GHz PC. The codes to regenerate the results can be accessed on ModelDB (Accession# 266941).

3. Results

3.1. Emergence of elevated beta rhythm in the primary motor cortex (M1)

Altering the synaptic connections both within and between cortex and thalamus, similar to the changes in synaptic strength identified by Reis *et al* [18], leads to the transition to a PD-like state, i.e. high beta rhythm in the simulated cortical LFP, along with highly synchronized activity of neurons across the TCM with silent periods of duration of the order of 1 s (figure 3(a)).

Enhanced synchrony among the populations of neurons in the TCM under PD conditions is evident, compatible with neural firing patterns, recorded across corticofugal projection neurons (CxFn) from 6-OHDA-lesioned rats [2]. The synaptic coupling changes that led to this are summarized in the normalized mean synaptic weights matrix, figure S1 (see the supplementary material). More specifically, the coupling strength between layers S to M in the cortex, TCR to TRN in the thalamus and corticothalamic connections were decreased, while the strength of connections from M to S in M1, TRN to TCR in thalamus and TC connections were increased. In addition to these changes, we increased the inhibitory couplings from CI to the deep layer of M1 (D), to achieve a PD-like condition that was more consistent with reported experimental recordings, in particular increased periods of silence and a level of synchronization in D layer neurons that is evident in the raster plot, figure 3(a). Increased neural inhibition has been experimentally identified as a factor potentially responsible for high amount of synchrony in M1 [9].

The corresponding simulated LFP signal, comprised of the summation of all EPSCs in layer D and inhibitory PSCs in CI is presented in figure 3(b) and its PSD in figure 3(c). Elevated activity in the beta frequency range is evident in the LFP power spectrum, consistent with the experimental recordings by Li *et al* [2] (figure 3(d)).

3.2. Addition of DBS to the PD state: suppression of the exaggerated beta rhythm

Following experimental evidence supporting an important role of the hyperdirect pathway in therapeutic effects of DBS through the antidromic activation of neurons within the deep layer of M1 [2, 9, 22, 47], we added DBS as intracellular inputs to a percentage of the PNs in layer D (hyperdirect neurons) as shown in figure 2.

130 Hz DBS was first added at an intensity that directly activated 25% of the layer D PNs with a fixed amplitude of the intracellularly injected pulse train ($A = 335$, see section 2) for 10 s, mimicking the antidromic activation of PNs via the hyperdirect pathway. Figures 4(a) and (b) illustrate the simulated raw and beta-band filtered LFPs of cortical layer D, respectively, during 10 s periods of DBS off and DBS on. DBS onset is at 10 s, however, the reduction in amplitude of the LFP signal in beta band (figure 4(b)) is reduced gradually over ~2 s due to short-term synaptic plasticity included in the model, hypothesized to be an important component of therapeutically beneficial high-frequency DBS [42]. Similarly, at DBS offset at 20 s, the increase in beta power gradually occurs over ~2 s. The frequency content of the LFP signal is presented in the corresponding PSD during the first 10 s (DBS off) and second 10 s (DBS on) in figures 4(c) and (d), for the raw and beta filtered LFP signals, respectively.

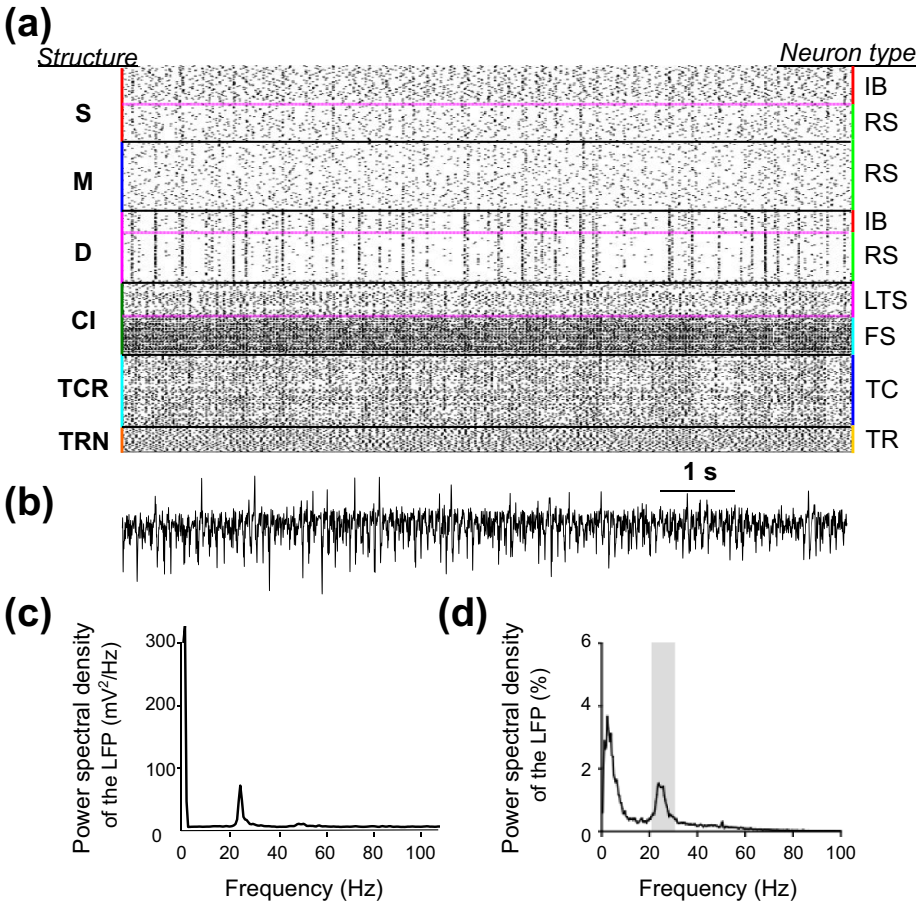

Figure 3. (a) Raster plot of the TCM neurons shown in different structures for 10 s under PD conditions. The populations and subpopulations are separated by bold black and pink horizontal lines, respectively. (b) Simulated LFP in D layer. (c) Power spectral density of the simulated LFP shown in (b) and (d) LFP recorded from deep layer of the motor cortex in 6-OHDA-lesioned parkinsonian rat (Reprinted from [2], Copyright (2012), with permission from Elsevier.).

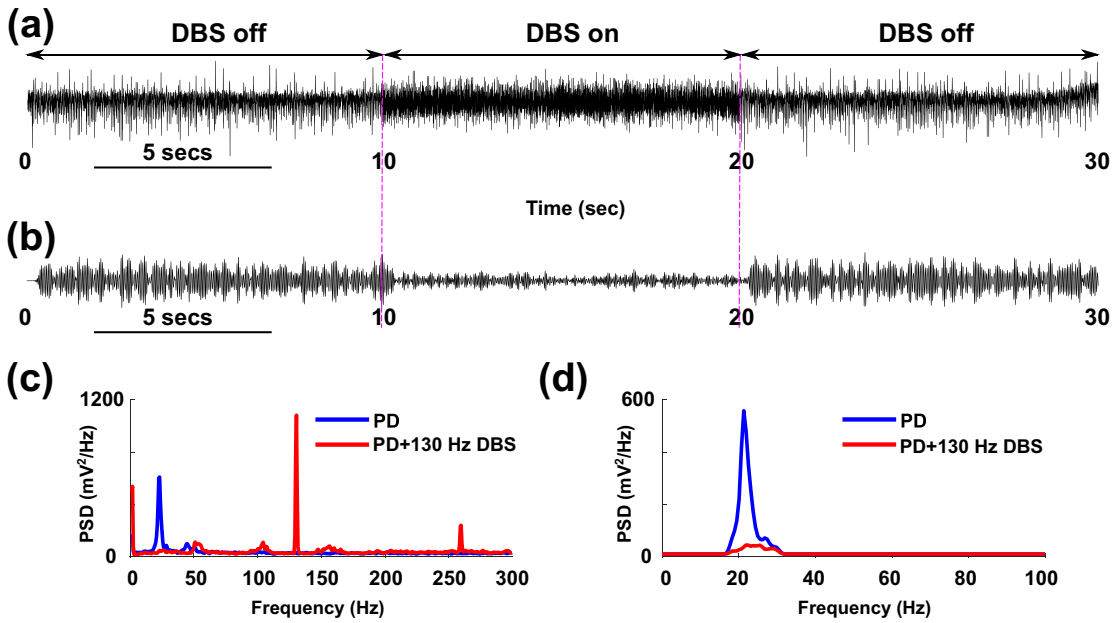

Figure 4. (a) Simulated LFP from cortical layer D for 30 s with 10 s periods of DBS off, DBS on and DBS off. (b) The band-pass filtered LFP signal in (a) filtered around the beta rhythm (13–30 Hz). (c) The power spectral density of the first 10 s of the LFP in (a) (blue) indicates exaggerated beta power that is suppressed by high frequency DBS at 130 Hz, applied from 10 to 20 s (red). (d) The power spectral sensity similar to that shown in (c) for the beta-band filtered LFP. The DBS intensity is set to activate 25% of the PNs in layer D.

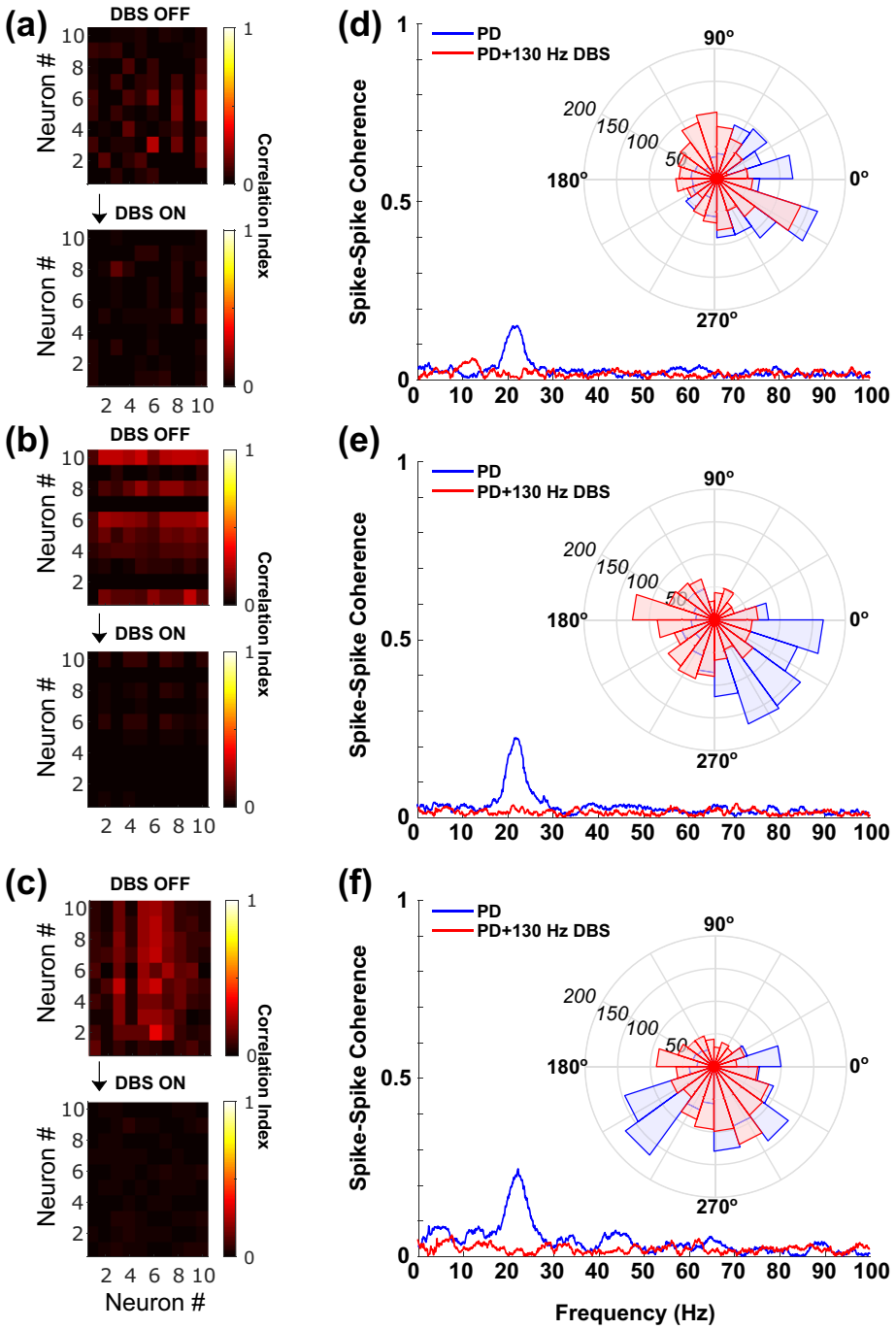

Figure 5. Cross-correlation diagrams for ten randomly chosen PNs between (a) M and S layers (b) M and D layers and (c) D and S layers during off and on DBS. The diagrams during DBS ON are presented for the same pairs of neurons during DBS OFF. The magntidue and phase of the cumulative spike-spike coherence between mutual layers are shown in (d) for M and S, (e) M and D and (f) D and S layers. The peak in the magnitude of coeherence between cumulative spikes in PD-like condition shows that the spikes between the corresponding layers are more coherent in beta band. The phase diagrams confirm that the phase delays between spikes of mutual layers are synchronized in PD-like condition (the blue histograms) and desynchronized by high frequency DBS (the red histograms).

3.3. Desynchronization of cortical motor network activity by high frequency DBS

In the same simulation set as in the previous subsection (figure 4), the cross-correlation between ten arbitrarily chosen pairs of neurons in layers S-M, M-D and S-D, was estimated and is presented in figures 5(a)–(c), respectively, during DBS on and DBS off.

The correlation between pairs of neurons in all cases was reduced by the application of high frequency (130 Hz) DBS to the layer V neurons, indicating that DBS desynchronizes the highly correlated activity of neuronal pairs in M1. The frequency range at which this correlation occurs is evident in the spike-spike coherence between cumulative spike trains from different cortical layers shown in figures 5(d)–(f) for

S-M, M-D and S-D, respectively. In all three cases, higher coherence in the beta rhythm range in the PD-like state (blue curves) was reduced during application of 130 Hz DBS (red curves). The phase of spike-spike coherence is presented in polar phase diagrams in the inset of figures 5(d)–(f), that can be interpreted as a measure of phase-locking between the spikes. It can be seen that the majority of spikes that are coherent with each other are localized within certain phase ranges in the PD-like condition (blue phase histograms), while application of DBS spreads the phase of the coherent activity across the range (red phase histograms). In PD-like condition, layer S and M neurons are coherent with relative phase between −60 and 30 degrees. Application of DBS causes a reduction in coherence with phase randomly distributed across the total phase range (0–360 degrees), figure 5(d). A similar phenomenon is observed between layers M and D (figure 5(e)), where neuron spikes are typically coherent with relative phase between −90 and 0 degrees. Finally, coherence was observed between layers S and D spikes with relative phase distributed between −160 and −30 degrees, figure 5(f).

The observed desynchronization of M1 activity is supported by experimental results, where strong correlations between neurons disappeared with the application of high frequency STN DBS in 6-OHDA-lesioned rats [2].

3.4. Antidromic activation of M1, excitation and suppression of cortical activity

The transmembrane potentials of ten arbitrary layer D neurons that were directly stimulated by DBS were examined during DBS off and DBS on, figure 6(a), with the same simulation settings as before. Antidromic activation of these neurons led to an increase in their mean firing rate from 3 ± 2 Hz (with DBS off) to 35 ± 5 Hz (during DBS on). This increase is consistent with reported values for mean firing rates of layer V pyramidal tract neurons during DBS on and off, in 6-OHDA-lesioned rats [2], 2.54 ± 0.17 Hz while DBS was off and 32 ± 5 Hz during 125 Hz DBS. The level of net inhibition throughout the cortex in the PD-like state had a large contribution in limiting the increase in firing rate during DBS to approximately 30–40 Hz, as observed by Li *et al* [2]. In the absence of high levels of inhibition, the firing rate of the hyperdirect neurons increased above the experimentally observed range, approaching the DBS frequency (data not shown). Figure 6(b) illustrates examples of PNs in layer D that were indirectly activated by DBS, i.e. neurons in layer D that received PSCs in response to DBS. With DBS off (left) the mean firing rate of these PNs was 4 ± 1 Hz. During DBS (right) both excitation and suppression of these neurons was observed, compatible with experimental recordings in primates [28]. To examine whether the suppression and excitation of these PNs depends on DBS intensity, the percentage of directly activated neurons in layer D was increased from 10% to 25% and then 50%, figure 6(c) (1, 2 and 3). At low DBS intensity (figure 6(c1)) all indirectly activated neurons were excited and no suppression of neural firing was observed. However, as the number of directly activated neurons was increased, a higher proportion of neurons within the network tended to be suppressed, figures 6(c2) and (c3). These results are of particular interest since the heterogeneous effects of antidromic activation of cortical PNs is a potential cellular mechanism by which STN DBS can disrupt exaggerated cortical beta activity.

3.5. Effect of DBS frequency on the spectral content of the simulated M1 LFP

With 50% of layer D neurons directly activated during DBS, the DBS frequency was varied and the power spectrum of the simulated cortical LFP computed, to examine the effect of stimulation frequency on the beta rhythm in the M1 LFP. The PSDs of LFPs during 10 s epochs of PD and DBS on states were estimated and are illustrated in figure 7 for DBS frequencies of 10, 25, 50, 100, 130, 160 and 200 Hz. The interplay between the DBS frequency and the beta oscillations generated intrinsically within the network is evident as seen in the spectra presented in figures 7(a)–(g). Specifically, harmonics of the DBS fundamental frequency emerge within the power spectrum when the DBS frequency is set below 50 Hz. For high frequency DBS, the level of suppression of the exaggerated beta rhythm increased with increasing DBS frequency, figures 7(h)–(n), with complete suppression of beta oscillations occurring at frequencies of approximately 130 Hz and above. This is consistent with clinical and experimental studies that suggest 130 Hz to be a preferred frequency for clinically therapeutic DBS [48, 49], knowing that there is not necessarily a correlation between excessive beta power in M1 and symptoms in PD patients. In addition, new rhythmic activity emerged within the LFP at intermediate frequencies between approximately 45 Hz and 70 Hz (figures 7(d)–(g)).

When the amplitude of the intercellular DBS current to the PNs was increased, peaks in the power spectrum of the cortical LFPs emerged at subharmonics of the DBS frequency in the gamma frequency range, figures 8(b)–(d). The emergence of these subharmonics depended on the strength of the stimulus and synaptic inputs, and on the net excitation-inhibition in the network. Figure 8(a) highlights the amplitude of the intracellular DBS current (parameter A in equation (1), see section 2) at which subharmonics of the DBS frequency were generated in the cortical LFP for a range of DBS frequencies. The examples in figures 8(b)–(d) show the PSD of the simulated LFPs during 130, 150 and 160 Hz DBS, and the generation of subharmonics at 65, 75 and

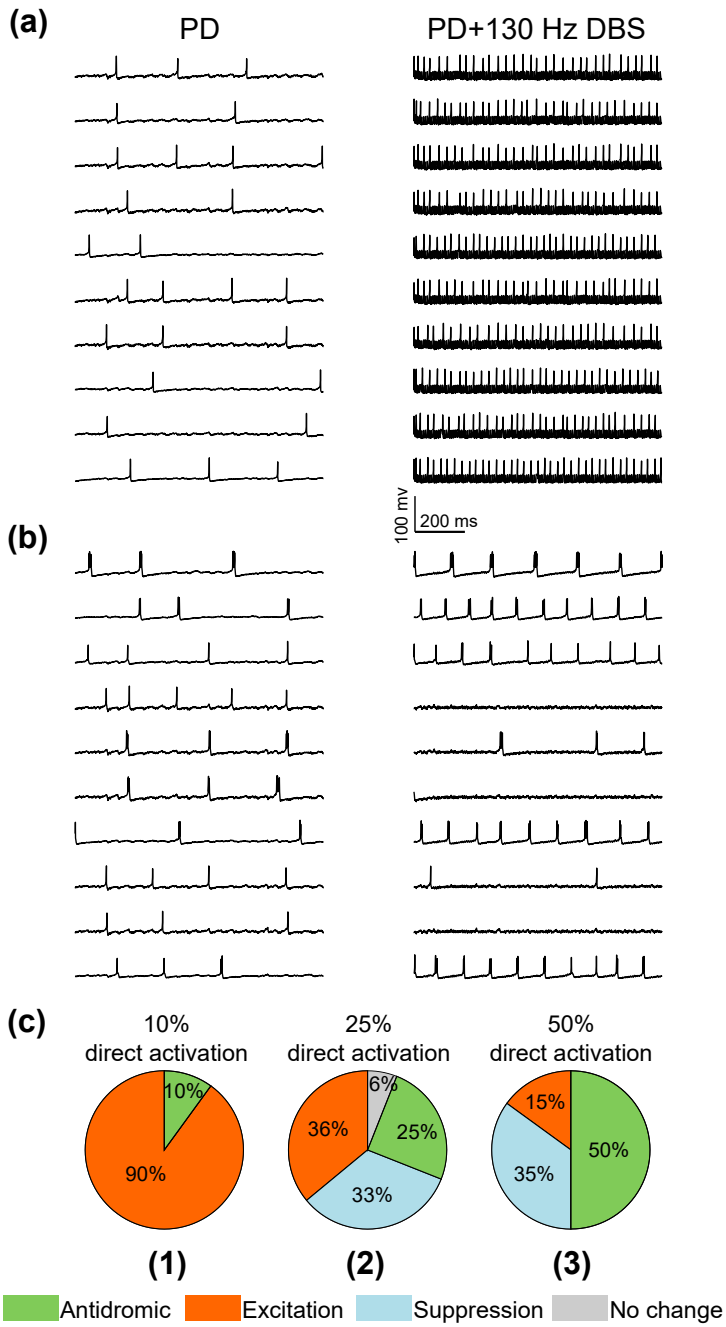

Figure 6. (a) The transmembraine potentals of ten randomly chosen PNs antidromically activated in PD condition (left column) and during 130 Hz DBS (right). (b) The transmembrane potentials as shown in (a) for other PNs in the deep cortical layer that were not directly activated by DBS. (c) The proportion of deep layer PNs excited, inhibited or with no change in mean firing rate varied with stimulation intensity; (1) 10%, (2) 25% and (3) 50% of the PNs are considered to be directly activated by DBS at 130 Hz.

80 Hz, respectively. The PSD of the PN spike trains for both hyperdirect and non-hyperdirect PNs in layer D revealed that both types of PNs were entrained to the DBS frequency at 130 Hz at high amplitudes of intracellular stimulation ($A \geq 520$), however in the other regime, while hyperdirect PNs remained entrained to the stimulus frequency, other neurons were partially entrained or modulated by the stimulus resulting in a peak in the power spectrum at half of the fundamental DBS frequency (i.e. at 65 Hz for 130 Hz DBS). Similar behavior was observed across the range of DBS frequencies examined.

3.6. Effect of DBS intensity and frequency on the attenuation of beta rhythm in M1

The time evolution of the PSD (spectrogram) of the simulated LFP is presented in figure 9(a) for 130 Hz DBS alternating between on and off DBS in 6 s epochs. The effect of the extent of DBS activation of layer D neurons was examined by varying the percentage of deep cortical PNs directly activated by the stimulation. Data are presented for 5%, 10%, 25%, 50% and 100% direct activation of PNs. A key feature of the presented TCM model is the inclusion of short term synaptic plasticity through TM

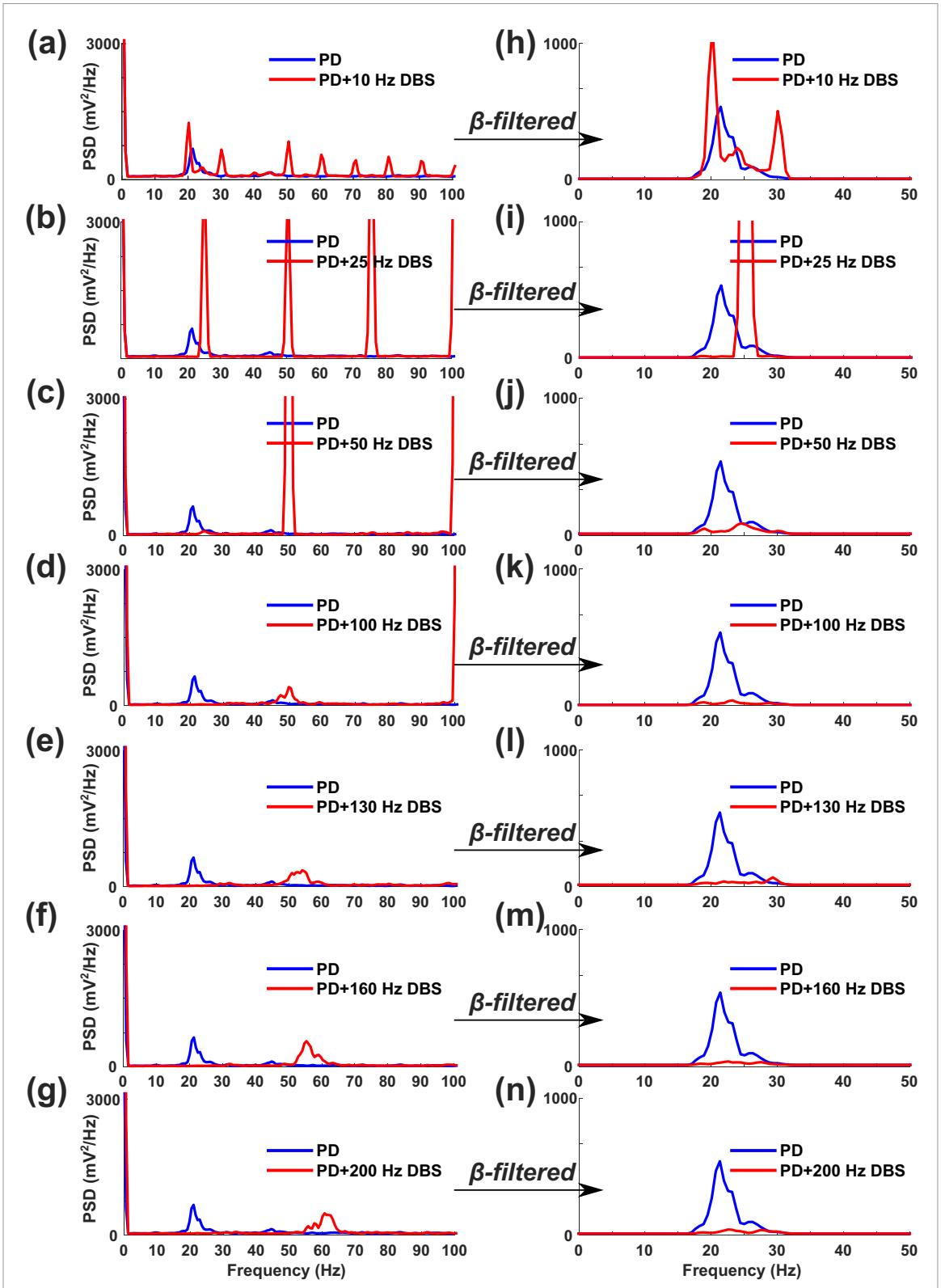

Figure 7. (a)–(g) Power spectral density of LFPs for different DBS frequencies: 10, 25, 50, 100, 130, 160 and 200 Hz, respectively. (h)–(n) the corresponding beta filtered PSDs. 50% of layer D neurons are directly activiated by DBS.

synapses, resulting in a gradual suppression and reemergence of beta band oscillations at DBS on/offset, figure 9(a). Consequently, the beta oscillations reappear after ∼2 s of turning DBS off.

As the extent of DBS activation of PNs increased, low gamma oscillations become not only more dominant, but also shifted towards higher frequencies, figure 9(a), similar to the effect observed when increasing the frequency of stimulation, figures 7(d)–(g).

Having separately investigated the effects of frequency and intensity of stimulation on cortical

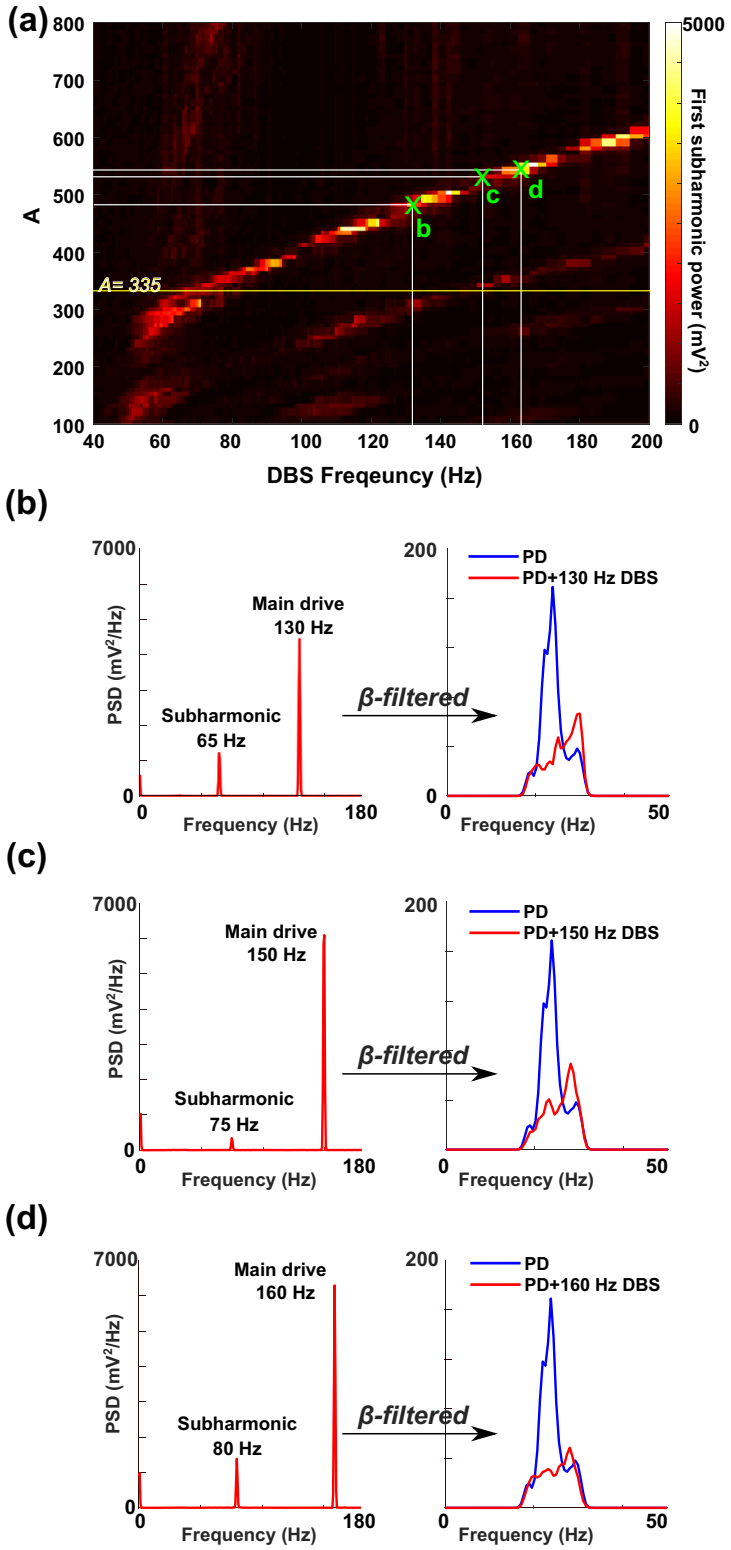

Figure 8. (a) The power of the first DBS subharmonic in the simulated M1 LFP represented as a heatmap for different values of DBS frequency and intensity (see section 2.2). All simulations presented, other than those in this subsection and figure were performed for $A = 335$, shown by a yellow horizontal line. (b)–(d) Examples of M1 LFP PSD at different DBS frequencies 160, 130 and 150 Hz, respectively, with variable DBS amplitude (parameter A) to obtain first DBS subharmonic. These examples correspond to the indicated points b, c and d in (a). The corresponding beta-filtered PSDs are shown on the right side. 25% of layer D neurons were directly stimulated by DBS.

network effects, the combined effect of simultaneously varying both on the attenuation of pathological cortical beta rhythms was then investigated. The beta power in the power spectrum of the simulated M1 LFPs was calculated for different DBS frequencies from 10 to 200 Hz, each for 10 s, and repeated for different intensities of DBS by varying the percentage of activated hyperdirect neurons, figure 9(b).

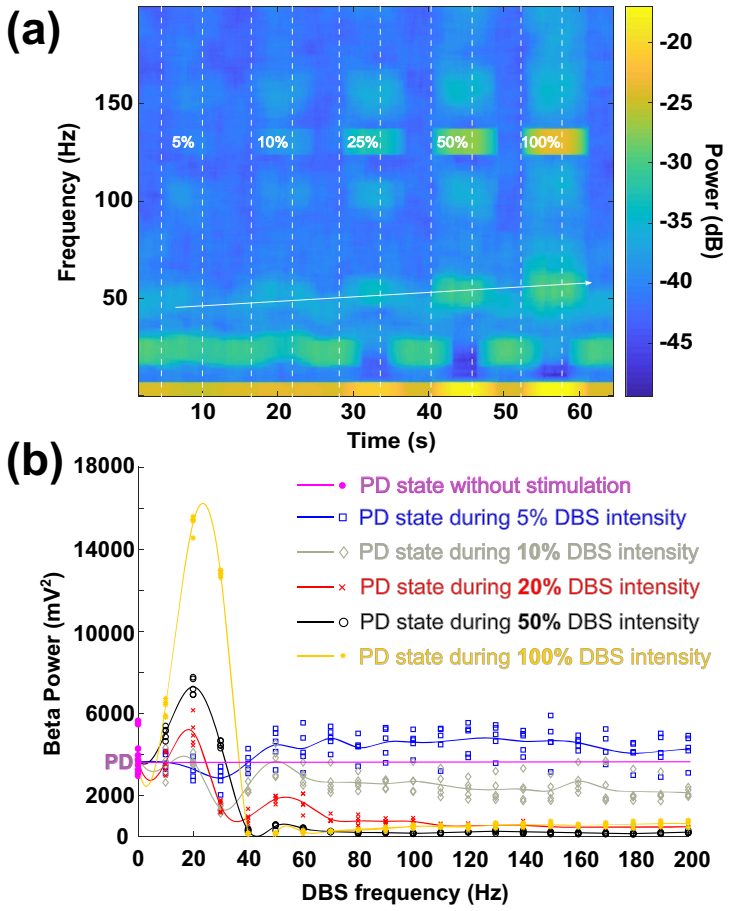

Figure 9. (a) Spectrogram of the M1 LFP during off/on DBS states, 5 s each interval. The intensity of DBS in each on DBS intevral was changed to make a comparison at a fixed DBS frequency, 130 Hz. 5%, 10%, 25%, 50%, and 100% of the PNs of cortical layer D were directly stimulated in the TCM model. The variance of stimulated PNs in the deep layer of the motor cortex is equivalent to altering the strength of the extracellular electric field induced by the DBS electrode. DBS gradually suppresses the beta band oscillations at the onsets. The white dashed lines indicate the on/offsets of DBS. The beta oscillations reappear after a few seconds of turning DBS off for each interval. The white tilted arrow shows the gradual shift in frequency of the low gamma oscillations. (b) The beta power in the M1 LFP during DBS at different frequencies and with increasing activation of the layer D neurons. Five trials were conducted at each frequency and intensity and the curves fitted using a cubic spline.

At low intensities of DBS that directly activated only 5% of PNs in layer D (blue squares and curve), DBS acts as a weak perturbation that amplified beta band power at stimulation frequencies above ∼50 Hz, and disrupts the beta band activity at frequencies lower than ∼50 Hz. This can be speculated as the weak entrainment of some neurons within the network to the DBS drive and high level of nonlinearity in the TCM. This phenomenon was not observed at DBS intensities higher than 5%, where the beta band power had direct relationship with the DBS intensity at frequencies lower than ∼50 Hz. Interestingly, direct activation of only 10% of the deep cortical PNs resulted in a halving of the initial beta power at stimulation frequencies higher than 100 Hz (gray diamonds and curve). The increase of hyperdirect neuron activation from 10% to 20% suppressed the beta power almost completely at high frequencies (red crosses and curve), similar to what is observed at 50% (black circles and curve) and even 100% activation (yellow stars and curve). These findings help explain how antidromic activation of deep layer PNs with 130 Hz DBS, within a specific intensity range, is particularly effective at suppressing high levels of beta activity in the motor cortex. The case of low frequency stimulation (lower than 30 Hz) suggests that stimulation of the TCM network at frequencies within the beta range, leads to an increase in beta power (except for very low DBS intensity), an undesirable outcome of the system related to resonance within the network. Driving the network with the same (or almost near) the natural frequency of oscillations, amplifies these oscillations and with potentially undesirable effects, especially at higher stimulation intensities, figure 9(b).

4. Discussion

4.1. TCM model

The role of DBS in modulating cortical activity in PD is not yet fully understood, although human and animal studies provide converging evidence that antidromic activation of cortical neurons through the

hyperdirect pathway can contribute to the therapeutic efficacy of DBS. Using a computational model of the TC microcircuit, we illustrate how antidromic activation of the hyperdirect pathway during STN DBS can alter neural activity throughout the cortical network, resulting in a range of phenomena including alteration of neural firing rates, suppression of beta activity, disruption of neural synchrony and the emergence of resonant harmonics.

The model of beta generation follows previous models of the cortex and thalamortical network which have investigated mechanisms underpinning the generation of beta activity within these structures [17, 18]. Sherman *et al* [17] examined beta emergence in the neocortex through interactions between laminar layers and integration of external synaptic drive, potentially from the thalamus, on the proximal and distal dendrites. The emergence of beta activity in our model similarly depends on the interaction between laminar layers of the cortex and thalamic inputs, however, as the model consists of point-like neurons it does not distinguish between distal and proximal inputs in contrast to multi-compartment neurons used in the aforementioned model. In accordance with the dynamic causal modelling study by Reis *et al* [18] our TCM model of simplified spiking neurons captures the main structures and connections of the cortex and thalamus that have been associated with the generation of pathological beta oscillations in PD and exhibits experimentally observed behavior in M1 recorded during DBS at both cellular and network levels. In addition, the spiking TCM model provides a simplified, yet realistic neuronal platform to implement arbitrary stimulation of desired structures within the thalamo-cortex and investigate their cortical network effects. In contrast to neural mass models, such as that presented by Reis *et al* [18], the spiking TCM model captures single neuron activity, enabling their ability to reproduce specific spiking patterns characteristic of cortical neural activity in PD, such as synchronization, bursting and entrainment to STN DBS, to be examined. Cortical effects of DBS on individual neural firing patterns and LFPs can thus be explored simultaneously. Network parameters were systematically adjusted to produce elevated beta rhythms in the cortical LFP, high neuronal synchronization in the primary motor cortex (figure 5), silent periods that match with experimental recordings and deep PNs firing rates [2]. In this way, the parameter space was constrained to design a model that captured DBS cortical effects such as suppression of exaggerated beta rhythm at high stimulation frequencies (figures 4 and 7), disruption of neural synchrony (figure 5) and the existence of both suppressed and excited clusters of neurons during optimum levels of DBS intensity (figure 6) [28]. The model system also exhibits a number of key phenomena including short-term synaptic suppression during high frequency DBS, resonance and elimination of low-frequency oscillations by high frequency perturbations that are also observed in physiological network behaviors.

4.2. Transition from non-parkinsonian to parkinsonian states

The coupling between nuclei in the normal (non-PD) state was initially set to generate physiological firing rates within the different populations across the TCM, with relatively low levels of beta rhythm within the network. Considering qualitative changes in couplings within and between thalamus and cortex identified experimentally using Bayesian inference [18], the network was gradually moved to a high beta state, by strengthening and weakening the synaptic couplings. The specific changes identified (originally by Reis *et al* [18]) were 1) an increase in the synaptic weight of the thalamic projections from TCR to D and CI, similarly from M to S and from TRN to TCR; 2) a decrease in the synaptic coupling between S to M in the cortex, between D to both nuclei of TCR and TRN and from TCR to TRN in thalamus. In addition, we increased inhibition from CI to D to better match our results with electrophysiological recordings [9]. Transitioning from non-PD to PD state introduced periods of silence up to greater than 1 s in the firing patterns across all populations along with exaggerated synchronization across populations (figure 3).

4.3. Propagation of DBS through the TCM: the role of synapses and interneurons

DBS stimuli invaded the cortical network initially by stimulating a percentage of PNs in layer D, representing direct activation of axons of the hyperdirect pathway. DBS subsequently affected other structures via synaptic connections from the hyperdirect PNs to a percentage of neurons in layer S, CIs, and two thalamic nuclei (figure 2). The indirect activation of other cells had a substantial contribution to the network modulating effects of DBS, including the observation of the DBS fundamental frequency in the PSD of individual neurons (data not shown). The network model thus follows the mechanism of propagation of signals through the cortical network that engages feedback and feedforward excitatory–excitatory and excitatory–inhibitory neuronal microcircuits [21]. The DBS signals that reach deep layers of the cortex antidromically propagate to superficial layers via excitatory synapses and return back to the PNs via synaptic connections in the opposite direction while at the same time are dampened by activation of interneurons with inhibitory synapses to the primary PNs.

Increasing the synaptic strength from CI to PNs, particularly in layer D, resulted in a more synchronized network, yielding raster plots similar to those observed in experimental recordings in parkinsonian rats [2], along with the formation of clusters of neurons in M1. This also allowed DBS to re-activate the

same CIs and modulate their firing times, resulting in the emergence of a peak in the CI power spectrum at 130 Hz while leaving the mean firing rates relatively unchanged. The mean firing rates of PNs in the cortex that were not directly stimulated were 1–4 Hz which is in the range of reported experimental data [2].

The existence of branch points from hyperdirect PNs to the CIs and also other structures within the TCM affected propagation of the DBS fundamental frequency through the network. In the model we included the branch point of the cortical PNs to cortical interneurons that has been suggested as a possible pathway mediating the therapeutic effects of DBS and altering the excitation inhibition balance [1, 9]. DBS modified the balance between excitatory and inhibitory neurons (the net excitation-inhibition balance in the network) in the model, in accordance with human studies that suggest DBS has a direct effect on intracortical neurons modulating cortical excitability in PD [50]. When branches from the descending axons to the interneurons were removed, the fundamental frequency was almost entirely suppressed in the PSD of the neurons spikes in different structures, except at unrealistically high intensities of DBS. Collectively, the simulation results indicate that modulation of cortical network activity by DBS in a manner consistent with experimental observations requires the postsynaptic DBS stimuli to reach CI, S layer and thalamic nuclei to varying extents. In particular, the model revealed that the propagation of the fundamental DBS frequency to other structures within the network depends on the synaptic mechanism and weights. The simulation results additionally add support to the hypothesis that activation of the CIs, both indirectly via postsynaptic DBS currents and as a result of synaptic connections in the TCM model, are an important aspect of cortical effects of DBS contributing to disruption of synchrony in the M1 network as previously suggested [1, 51, 52].

4.4. Cortical network effects of DBS: suppression of beta band oscillations and neural synchrony, resonance effects and emergence of DBS subharmonics

Low frequency stimulation led to further amplification of the beta rhythm in M1, while high frequency stimulation lowered the amplitude of beta activity in the PD state (figures 4 and 9(b)), consistent with previous optogenetics [26] and clinical studies [53]. The attenuation and amplification of beta activity depended on both DBS intensity and frequency (figure 9(b)).

An interplay between DBS and its subharmonics with existing cortical oscillations was observed in the model (figures 7 and 9(b)). Note that the emergence of new frequencies in nonlinear models such as the TCM model presented can be amplitude-dependent with the system exhibiting more complex oscillatory phenomena than that observed in simple linear systems. The emergence of resonant frequencies in cortical microcircuits activated by antidromic DBS have been identified in animal and human studies [21, 54] with suggested resonant mechanisms due to DBS that are patient specific and is invoked in cortico-subcortical loops [54].

While experimental results suggesting that DBS regulates neural firing may seem to be in contradiction with the desynchronization effect of DBS, unifying theoretical and numerical results potentially merge these two competing hypotheses by considering clusters of neuronal populations. Over short time scales these clusters can illustrate temporary entrainment to DBS and on a long time-scale manifest desynchronization [55]. The model exhibits both of these effects in different subpopulations: hyperdirect PNs that are entrained to the stimulus, with others activated by synaptic connections exhibiting disrupted synchronization (figures 5(d)–(f)).

Activating only 10% of the PNs in the deep layer of the cortex resulted in suppression of the beta rhythm by almost half (figure 9(a)). Direct activation of just 25% of the deep cortical PNs was sufficient to attenuate the beta rhythm in the cortical neurons by more than 80%. This was also observed for DBS that directly activated 50% of the PNs, however, was not the case for 100% activation, which may be intuitively surprising. These results (figure 9(a)) suggest that there is an optimum range of activation of cortical neurons by DBS which exerts a beneficial effect in terms of the suppression of pathological beta activity within the cortex. The results are consistent with 'dose dependent' suppression of cortical beta band oscillations during STN DBS in human subjects by Whitmer *et al* [5], who observed increased suppression of cortical beta oscillations with increasing DBS amplitude, with the level of suppression saturating at higher applied voltages.

Finally, the model offers an explanation for the emergence of peaks at subharmonics of the DBS frequency in the cortical LFP power spectrum, which have been observed experimentally during DBS induced dyskinesia [29]. In the model, within specific ranges of the net excitatory–inhibitory balance, the first subharmonic of the DBS emerges and can drive cortical activity, varying systematically with DBS frequency as observed in figure 8.

4.5. Model assumptions and limitations

Several assumptions have been made in the design of the model and simulation. As the focus of the present study was to investigate antidromic effects of DBS on cortical network activity in isolation, orthodromic effects were not considered. DBS can further influence activity of the cortical network through orthodromic activation via the cortico-thalamic-cortical pathway [19, 56]. An understanding of how these effects interact together is needed to fully understand the mechanisms of high frequency DBS. A major

challenge in understanding network effects of DBS is reconciling data and results recorded in different species and under different experimental paradigms. The TCM model was designed and tuned, based on rodent models available in the literature, though behavior evident in monkeys and human subjects was also demonstrated. The representation of the cortex was simplified to a three-layer structure with just a single population of inhibitory neurons.

For computational efficiency, the application of DBS was simplified such that antidromic stimulation of the point-like PNs in layer D was implemented using intracellular stimulation with Dirac delta functions. The number of PNs stimulated in this way was set as a model parameter. In practice this would be determined by the distribution of electric field surrounding the DBS electrode and its interaction with branching collaterals, with the number of neurons stimulated varying with DBS amplitude and pulse duration. The spatial distribution of neurons within the TCM was similarly not considered, and the LFP was approximated as the summation of all PSCs in layer D of the cortex and all of the inhibitory PSCs due to the CI neurons. All synapses were represented using TM synapses, which while capturing key behaviors such as vesicle dynamics, and extensively used in similar cortical models [40], represent a simplification of the range of glutamatergic and GABAergic synapses within the network. Finally, the TCM model presented is a noise driven system with high sensitivity to bias currents and noise. A more detailed model of the thalamus with nuclei receiving drive from the BG would extend the TCM model to one that is BG driven, rather than white noise driven which would be more physiologically realistic [57].

5. Conclusions

Converging evidence from human and animal studies indicate that modulation of cortical network activity due to antidromic activation may play a role in the therapeutic efficacy of STN DBS for PD. The model presented illustrates how antidromic activation of cortical neurons during STN DBS modulates cortical network activity, with synaptic mechanisms playing a crucial role in frequency modulation, gating the propagation of stimulation throughout the network. The direct activation of deep PNs in M1 and subsequent indirect activation of other parts of the thalamo-cortical network via intracortical, cortico-thalamic and TC synaptic interactions were shown to mediate the influence of DBS on the cortex via the hyperdirect pathway. The results are consistent with experimental observations including suppression of beta activity during high frequency DBS, the emergence of resonant activity and desynchronization. Under certain conditions, increased LFP power was observed at subharmonics of the DBS fundamental frequency, consistent with observations in human subjects during DBS dyskinesia. By providing insight into the mechanisms underpinning these phenomena, computational modelling can improve understanding of these effects and contribute to the identification of more effective and less-invasive stimulation paradigms.

Data availability statement

The data that support the findings of this study are openly available at the following URL/DOI: https://senselab.med.yale.edu/modeldb/.

Acknowledgments

This work was supported by European Research Council (ERC) under the European Union's Horizon 2020 research and innovation programme (ERC-2014-CoG 646923-DBSModel).

Neuromuscular Systems Lab, School of Electrical & Electronic Engineering, University College Dublin, Ireland.

ORCID iDs

AmirAli Farokhniaee https://orcid.org/0000-0002-9653-0158
Madeleine M Lowery https://orcid.org/0000-0001-6743-360X

References

[1] Arbuthnott G W and Garcia-Munoz M 2017 Are the symptoms of parkinsonism cortical in origin? *Comput. Struct. Biotechnol. J.* **15** 21–5
[2] Li Q, Ke Y, Chan D C W, Qian Z M, Yung K K L, Ko H, Arbuthnott G and Yung W H 2012 Therapeutic deep brain stimulation in parkinsonian rats directly influences motor cortex *Neuron* **76** 1030–41
[3] Sharott A, Magill P J, Harnack D, Kupsch A, Meissner W and Brown P 2005 Dopamine depletion increases the power and coherence of β-oscillations in the cerebral cortex and subthalamic nucleus of the awake rat *Eur. J. Neurosci.* **21** 1413–22
[4] De Hemptinne C, Swann N C, Ostrem J L, Ryapolova-Webb E S, San Luciano M, Galifianakis N B and Starr P A 2015 Therapeutic deep brain stimulation reduces cortical phase-amplitude coupling in Parkinson's disease *Nat. Neurosci.* **18** 779–86
[5] Whitmer D, De Solages C, Hill B, Yu H, Henderson J M and Bronte-Stewart H 2012 High frequency deep brain stimulation attenuates subthalamic and cortical rhythms in Parkinson's disease *Front. Hum. Neurosci.* **6** 1–18
[6] Crowell A L, Ryapolova-Webb E S, Ostrem J L, Galifianakis N B, Shimamoto S, Lim D A and Starr P A 2012 Oscillations in sensorimotor cortex in movement disorders: an electrocorticography study *Brain* **135** 615–30
[7] Pollok B, Krause V, Martsch W, Wach C, Schnitzler A and Südmeyer M 2012 Motor-cortical oscillations in early stages of Parkinson's disease *J. Physiol.* **590** 3203–12
[8] Weiss D *et al* 2015 Subthalamic stimulation modulates cortical motor network activity and synchronization in Parkinson's disease *Brain* **138** 679–93

[9] Li Q, Qian Z M, Arbuthnott G W, Ke Y and Yung W H 2014 Cortical effects of deep brain stimulation implications for pathogenesis and treatment of parkinson disease *JAMA Neurol.* **71** 100–3
[10] Scholten M *et al* 2016 Cortical correlates of susceptibility to upper limb freezing in Parkinson's disease *Clin. Neurophysiol.* **127** 2386–93
[11] Holt A B and Netoff T I 2014 Origins and suppression of oscillations in a computational model of Parkinson's disease *J. Comput. Neurosci.* **37** 505–21
[12] Nevado Holgado A J, Terry J R and Bogacz R 2010 Conditions for the generation of beta oscillations in the subthalamic nucleus-globus pallidus network *J. Neurosci.* **30** 12340–52
[13] McCarthy M M, Moore-Kochlacs C, Gu X, Boyden E S, Han X and Kopell N 2011 Striatal origin of the pathologic beta oscillations in Parkinson's disease *Proc. Natl Acad. Sci. USA* **108** 11620–5
[14] Santaniello S, McCarthy M M, Montgomery E B, Gale J T, Kopell N and Sarma S V 2015 Therapeutic mechanisms of high-frequency stimulation in Parkinson's disease and neural restoration via loop-based reinforcement *Proc. Natl Acad. Sci. USA* **112** E586–95
[15] Kumaravelu K, Brocker D T and Grill W M 2016 A biophysical model of the cortex-basal ganglia-thalamus network in the 6-OHDA lesioned rat model of Parkinson's disease *J. Comput. Neurosci.* **40** 207–29
[16] Lindenbach D and Bishop C 2013 Critical involvement of the motor cortex in the pathophysiology and treatment of Parkinson's disease *Neurosci. Biobehav. Rev.* **37** 2737–50
[17] Sherman M A, Lee S, Law R, Haegens S, Thorn C A, Hämäläinen M S, Moore C I and Jones S R 2016 Neural mechanisms of transient neocortical beta rhythms: converging evidence from humans, computational modeling, monkeys, and mice *Proc. Natl Acad. Sci.* **113** E4885–94
[18] Reis C, Sharott A, Magill P J, Bcm V W, Parr T, Zeidman P, Friston K J and Cagnan H 2019 Thalamocortical dynamics underlying spontaneous transitions in beta power in Parkinsonism *Neuroimage* **1** 103–14
[19] Kumaravelu K, Oza C S, Behrend C E and Grill W M 2018 Model-based deconstruction of cortical evoked potentials generated by subthalamic nucleus deep brain stimulation *J. Neurophysiol.* **120** 662–80
[20] Devos D *et al* 2004 Subthalamic nucleus stimulation modulates motor cortex oscillatory activity in Parkinson's disease *Brain* **127** 408–19
[21] Li S, Arbuthnott G W, Jutras M J, Goldberg J A and Jaeger D 2007 Resonant antidromic cortical circuit activation as a consequence of high-frequency subthalamic deep-brain stimulation *J. Neurophysiol.* **98** 3525–37
[22] Dejean C, Hyland B and Arbuthnott G 2009 Cortical effects of subthalamic stimulation correlate with behavioral recovery from dopamine antagonist induced akinesia *Cereb. Cortex* **19** 1055–63
[23] Kuriakose R *et al* 2010 The nature and time course of cortical activation following subthalamic stimulation in Parkinson's disease *Cereb. Cortex* **20** 1926–36
[24] Kang G and Lowery M M 2013 Interaction of oscillations, and their suppression via deep brain stimulation, in a model of the cortico-basal ganglia network *IEEE Trans. Neural. Syst. Rehabil. Eng.* **21** 244–53
[25] Anderson R W, Farokhniaee A, Gunalan K, Howell B and McIntyre C C 2018 Action potential initiation, propagation, and cortical invasion in the hyperdirect pathway during subthalamic deep brain stimulation *Brain Stimul.* **11** 1140–50
[26] Gradinaru V, Mogri M, Thompson K R, Henderson J M and Deisseroth K 2009 Optical deconstruciton of parkinsonian neural circuitry *Science* **324** 2005–8
[27] Yu C, Cassar I R, Sambangi J and Grill W M 2020 Frequency-specific optogenetic deep brain stimulation of subthalamic nucleus improves parkinsonian motor behaviors *J. Neurosci.* **40** 4323–34
[28] Johnson L A, Wang J, Nebeck S D, Zhang J, Johnson M D and Vitek J L 2020 Direct activation of primary motor cortex during subthalamic but not pallidal deep brain stimulation *J. Neurosci.* **40** 2480–19
[29] Swann N C, De Hemptinne C, Miocinovic S, Qasim S, Wang S S, Ziman N, Ostrem J L, San Luciano M, Galifianakis N B and Starr P A 2016 Gamma oscillations in the hyperkinetic state detected with chronic human brain recordings in Parkinson's disease *J. Neurosci.* **36** 6445–58
[30] Rubin J E and Terman D 2004 High frequency stimulation of the subthalamic nucleus eliminates pathological thalamic rhythmicity in a computational model *J. Comput. Neurosci.* **16** 211–35
[31] McIntyre C C, Grill W M, Sherman D L and Thakor N V 2004 Cellular effects of deep brain stimulation: model-based analysis of activation and inhibition *J. Neurophysiol.* **91** 1457–69
[32] Yamawaki N, Borges K, Suter B A, Harris K D and Shepherd G M G 2014 A genuine layer 4 in motor cortex with prototypical synaptic circuit connectivity *Elife* **3** e05422
[33] Yamawaki N and Shepherd G M G 2015 Synaptic circuit organization of motor corticothalamic neurons *J. Neurosci.* **35** 2293–307
[34] Bhatt M B *et al* 2016 Computational modelling of movement-related beta-oscillatory dynamics in human motor cortex *Neuroimage* **133** 224–32
[35] Shepherd G and Grillner S (eds) 2018 *Handbook of Brain Microcircuits* 2nd edn (Oxford : Oxford University Press)
[36] Douglas R J and Martin K A C 2004 Neuronal circuits of the neocortex *Annu. Rev. Neurosci.* **27** 419–51
[37] Traub R D, Contreras D, Cunningham M O, Murray H, Fen L, Roopun A, Bibbig A, Wilent W B, Higley M J and Whittington M A 2005 Single-column thalamocortical network model exhibiting gamma oscillations, sleep spindles, and epileptogenic bursts *J. Neurophysiol.* **93** 2194–232
[38] Izhikevich E M 2003 Simple model of spiking neurons *IEEE Trans. Neural Networks* **14** 1569–72
[39] Tsodyks M V and Markram H 1997 The neural code between neocortical pyramidal neurons depends on neurotransmitter release probability *Proc. Natl Acad. Sci.* **94** 719–23
[40] Markram H *et al* 2015 Reconstruction and simulation of neocortical microcircuitry *Cell* **163** 456–92
[41] Kang G and Lowery M M 2014 Effects of antidromic and orthodromic activation of STN afferent axons during DBS in Parkinson's disease: a simulation study *Front. Comput. Neurosci.* **8** 32
[42] Farokhniaee A and McIntyre C C 2019 Theoretical principles of deep brain stimulation induced synaptic suppression *Brain Stimul.* **12** 1402–9
[43] Lindén H, Tetzlaff T, Potjans T C, Pettersen K H, Grün S, Diesmann M and Einevoll G 2011 Modeling the spatial reach of the LFP *Neuron* **72** 859–72
[44] Latikka 2001 Physics in medicine and biology conductivity of living intracranial tissues conductivity of living intracranial tissues
[45] Hashemi M, Hutt A, Hight D and Sleigh J 2017 Anesthetic action on the transmission delay between cortex and thalamus explains the beta-buzz observed under propofol anesthesia *PLoS ONE* **12** e0179286
[46] Purpura K P and Chronux B H 2008 Neural signal processing toolbox *Tutorial*
[47] Sanders T H 2016 Phase-amplitude coupling, an indication of bursting in parkinsonism, is masked by periodic pulses *J. Neurophysiol.* **115** 1587–95
[48] Breit S, Schulz J B and Benabid A L 2004 Deep brain stimulation *Cell Tissue Res.* **318** 275–88
[49] Kuncel A M and Grill W M 2004 Selection of stimulus parameters for deep brain stimulation *Clin. Neurophysiol.* **115** 2431–41

[50] Fraix V, Pollak P, Vercueil L, Benabid A-L and Mauguiere F 2008 Effects of subthalamic nucleus stimulation on motor cortex excitability in Parkinson's disease *Clin. Neurophysiol.* **119** 2513–8
[51] Goldberg J A, Boraud T, Maraton S, Haber S N, Vaadia E and Bergman H 2002 Enhanced synchrony among primary motor cortex neurons in the 1-methyl-4-phenyl-1,2,3,6-tetrahydropyridine primate model of Parkinson's disease *J. Neurosci.* **22** 4639–53
[52] Carron R, Filipchuk A, Nardou R, Singh A, Michel F J, Humphries M D and Hammond C 2014 Early hypersynchrony in juvenile PINK1-/-motor cortex is rescued by antidromic stimulation *Front. Syst. Neurosci.* **8** 1–12
[53] Follett K A *et al* 2010 Pallidal versus subthalamic deep-brain stimulation for Parkinson's disease *N. Engl. J. Med.* **362** 2077–91
[54] Blumenfeld Z, Velisar A, Koop M M, Hill B C, Shreve L A, Quinn E J, Kilbane C, Yu H, Henderson J M and Brontë-Stewart H 2015 Sixty hertz neurostimulation amplifies subthalamic neural synchrony in Parkinson's disease *PLoS One* **10** 1–12
[55] Wilson D and Moehlis J 2015 Clustered desynchronization from high-frequency deep brain stimulation ed Diedrichsen J *PLoS Comput. Biol.* **11** e1004673
[56] Anderson C J, Sheppard D T, Huynh R, Anderson D N, Polar C A and Dorval A D 2015 Subthalamic deep brain stimulation reduces pathological information transmission to the thalamus in a rat model of parkinsonism *Front. Neural Circuits* **9** 1–11
[57] Kerr C C, Van Albada S J, Neymotin S A, Chadderdon G L, Robinson P A and Lytton W W 2013 Cortical information flow in Parkinson's disease: a composite network/field model *Front. Comput. Neurosci.* **7** 1–14